Available online at www.sciencedirect.com
SCIENCE DIRECT®
Journal of Computational Physics 208 (2005) 134–153
JOURNAL OF COMPUTATIONAL PHYSICS
www.elsevier.com/locate/jcp

Using stochastic analysis to capture unstable equilibrium in natural convection

Badrinarayanan Velamur Asokan, Nicholas Zabaras *

Materials Process Design and Control Laboratory, Sibley School of Mechanical and Aerospace Engineering, 188 Frank H.T. Rhodes Hall, Cornell University, Ithaca, NY 14853-3801, USA

Received 27 July 2004; received in revised form 27 January 2005; accepted 9 February 2005
Available online 14 April 2005

Abstract

A stabilized stochastic finite element implementation for the natural convection system of equations under Boussinesq assumptions with uncertainty in inputs is considered. The stabilized formulations are derived using the variational multiscale framework assuming a one-step trapezoidal time integration rule. The stabilization parameters are shown to be functions of the time-step size. Provision is made for explicit tracking of the subgrid-scale solution through time. A support-space/stochastic Galerkin approach and the generalized polynomial chaos expansion (GPCE) approach are considered for input–output uncertainty representation. Stochastic versions of standard Rayleigh–Bènard convection problems are used to evaluate the approach. It is shown that for simulations around critical points, the GPCE approach fails to capture the highly non-linear input uncertainty propagation whereas the support-space approach gives fairly accurate results. A summary of the results and findings is provided.

Keywords: Stochastic finite element method; Polynomial chaos; Askey-chaos; Variational multiscale method; Stabilized finite elements; Stochastic Galerkin method; Importance sampling; Natural convection

1. Introduction

Natural convection is started when the fluid buoyancy effect due to temperature gradients exceeds the stabilizing viscous effect [1]. The state where these opposing effects neutralize each other is called the first critical point (here denoted as CP1). Below CP1, the viscous effect dominates, the fluid flow is absent and heat transfer takes place by conduction. Above CP1, the buoyancy effect dominates, fluid-flow is initiated and heat transfer is by conduction and convection. When the system inputs fluctuate about CP1, the input–

* Corresponding author. Tel.: +1 607 255 9104; fax: +1 607 255 1222.
E-mail address: zabaras@cornell.edu (N. Zabaras).

0021-9991/$ - see front matter © 2005 Elsevier Inc. All rights reserved.
doi:10.1016/j.jcp.2005.02.007

output relationship becomes highly non-linear and possibly discontinuous due to the drastic change in the governing dynamics (convection above CP1 and conduction below). This observation leads us to the focus of this work: Can we capture the effect of input uncertainty on the flow and temperature patterns in natural convection (i) far from any critical points (Problem I) and (ii) when the input fluctuations are such that the system can be above and below CP1 with finite probabilities (Problem II).

In this work, we will use the generalized polynomial chaos expansion (GPCE) approach and the stochastic Galerkin/support-space method [2–9] for uncertainty propagation. The former uses polynomials from the Wiener–Askey family to represent the system outputs in terms of the uncertain system inputs. The latter employs finite element discretization of the support space of inputs (regions of strictly positive input joint probability density). The GPCE suffers in accuracy for highly non-linear input-to-output uncertainty propagation. This problem is not encountered with the support-space method. The common disadvantage of both approaches is the "curse of dimensionality", i.e., the computational cost increases exponentially as the inputs approach white noise. In this context, it is also worth mentioning that Le Maitre et al. [8] introduced the Wiener–Haar approach for addressing Problem II. Also, to the best of authors' knowledge, the stochastic Galerkin method and its variants have not been applied to natural convection problems.

In our previous work [10], we used the VMS approach [11–13] in conjunction with the generalized polynomial chaos for deriving stabilized finite element formulations for stochastic Navier–Stokes and stochastic advection-diffusion equations. We had assumed that the time-integration procedure does not affect the stabilization and that the subgrid scale/unresolved solution components are quasi-static stochastic processes and hence need not be tracked in time. These assumptions will be relaxed in the present work. In this respect, this paper is an extension of our previous work.

The layout of the paper is as follows. In Section 2 the preliminaries for mathematical representation of uncertainty are provided. The Boussinesq natural convection problem is defined in Section 3. The variational multiscale framework is used in Section 4 to derive the stabilized weak formulations for the natural convection equations. Section 5 then discusses some implementation issues for the above problem with regard to the GPCE and the support-space approaches. This is followed in Section 6 by two test examples corresponding to Problems I and II. A summary of findings is finally provided in Section 7.

2. Mathematical representation of uncertainty in physical systems

2.1. Mathematical preliminaries

A probability space is a triple $(\Omega, \mathscr{F}, \mathscr{P})$, where Ω is the sample space, $\mathscr{F}$ is the σ-algebra of subsets (events) of Ω and $\mathscr{P}$ is a probability measure on $\mathscr{F}$ [14]. A real-valued random variable is a function $X : \Omega \mapsto \mathbb{B}$, where $\mathbb{B}$ is a subset of the real line. In this paper, we will restrict ourselves to continuous random variables with cumulative distribution function (CDF) and probability density function (PDF) defined as follows:

$$F_X(x) := \mathscr{P}[X \leqslant x], \quad f_X(x) := \mathrm{d}F_X(x)/\mathrm{d}x, \tag{1}$$

where $F_X(x)$ and $f_X(x)$ denote the CDF and PDF of the random variable X, respectively. Throughout this paper, a random variable X will be denoted as $X(\omega)$, where ω denotes association with a probability space and is used to emphasize randomness in X.

The mathematical expectation of $X(\omega)$ can be defined using any of these equivalent forms

$$\mathbb{E}(X) := \int_\Omega X(\omega)\,\mathrm{d}\mathscr{P}(\omega) = \int_\Omega X(\omega)\mathscr{P}(\mathrm{d}\omega) = \int_{\mathbb{B}} xF_X(\mathrm{d}x) = \int_{\mathbb{B}} xf_X(x)\,\mathrm{d}x, \tag{2}$$

where $\mathbb{E}(\cdot)$ denotes the mathematical expectation operator.

The function space $L_2(\Omega)$ is defined as the space of all random variables $X(\omega)$ with $\mathbb{E}(|X(\omega)|^2) < \infty$. Further, $L_2(\Omega)$ is a Hilbert space with the inner-product between two random variables $X(\omega)$ and $Y(\omega)$ defined as their covariance [14]. Also, convergence in $L_2(\Omega)$ implies convergence in probability and convergence in distribution, i.e.

$$X_n \xrightarrow{L_2} X \Rightarrow \mathscr{P}[|X_n - X| \geqslant \epsilon] \to 0, \quad F_{X_n}(x) \to F_X(x), \text{ as } n \to \infty, \tag{3}$$

where $\epsilon > 0$ and convergence is in sup-norm. We will attempt to construct approximations to random variables and stochastic processes in the form of sequences that converge uniformly according to Eq. (3).

Remark 1. The definitions in this section can be generalized to vectors of random variables denoted as $\mathbf{X}(\omega) := (X_1(\omega), \ldots, X_m(\omega))$ and spatio-temporally varying random fields (*stochastic processes*) denoted as $W(\mathbf{x}, t, \omega)$.

2.2. Reduced modelling of stochastic processes

Theoretically, the stochastic process $W(\mathbf{x}, t, \omega)$ can be represented as a random variable at each spatial and temporal location. This requires infinite random variables (a computational impossibility) for complete characterization. Thus, we need techniques for reduced-order representation of stochastic processes. We will now briefly describe two most popular ways of approximating a L_2 (finite variance) stochastic process using a truncated series expansion comprised of a few random variables.

Karhunen–Loève expansion (KLE) [15,16]: Let $W(\mathbf{x}, t, \omega)$ be a L_2 stochastic process defined on a closed spatial domain $\mathscr{D}$ and a closed time interval $\mathscr{T}$. In short $\mathbb{E}(|W(\mathbf{x}, t, \omega)|^2) < \infty$ for all $\mathbf{x} \in \mathscr{D}$ and $t \in \mathscr{T}$. Then the KLE approximation of $W(\mathbf{x}, t, \omega)$ is defined as

$$W(\mathbf{x}, t, \omega) \approx W_N(\mathbf{x}, t, \omega) := \mathbb{E}(W(\mathbf{x}, t, \omega)) + \sum_{i=1}^{N} \sqrt{\lambda_i}\xi_i(\omega) f_i(\mathbf{x}, t), \tag{4}$$

where λ_i and $f_i(\mathbf{x}, t)$ are the eigenvalues and eigenfunctions of the covariance kernel $R_{\mathrm{WW}}(\{\mathbf{x}_1, t_1\}, \{\mathbf{x}_2, t_2\})$ of $W(\mathbf{x}, t, \omega)$ (see [16]) and $(\xi_1(\omega), \ldots, \xi_N(\omega))$ form a set of N independent random variables with an orthogonality relation $\mathbb{E}(\xi_m(\omega)\xi_n(\omega)) = \delta_{mn}$. Also, the joint PDF of $(\xi_1(\omega), \ldots, \xi_N(\omega))$ depends on the nature of $W(\mathbf{x}, t, \omega)$.

Remark 2. In practice, N is taken to be a sufficiently small number and is referred to as the KL dimension or the input dimensionality.

In order to define the KLE in Eq. (4), an a priori knowledge of the covariance kernel is required. This information is not available for the outputs of a continuum system (often solutions of a system of stochastic partial differential equations (SPDEs)). Hence, in the GPCE approach, we look for a suitable trial basis comprised of polynomials in L_2-random variables such that $W(\mathbf{x}, t, \omega)$ can be represented as a sum of its projections on the trial basis [2].

Generalized polynomial chaos expansion [3,4]: Here, any L_2-stochastic process (typically an output quantity) is represented in terms of a trial basis for $L_2(\Omega)$ consisting of hypergeometric orthogonal polynomials from the Askey series [2]. The truncated GPCE of an output random variable $X(\omega)$ belonging to $L_2(\Omega)$ as a function of $\boldsymbol{\xi} := (\xi_1(\omega), \ldots, \xi_N(\omega))^{\mathrm{T}}$ (see Eq. (4)) can be written as

$$X(\omega) \overset{L_2}{\approx} X_N(\omega) \overset{L_2}{=} a_0 I_0 + \sum_{i_1=1}^{N} a_{i_1} I_1(\xi_{i_1}(\omega)) + \cdots + \sum_{i_1=1}^{N} \cdots \sum_{i_n=1}^{i_{n-1}} a_{i_1 i_2 \ldots i_n} I_n(\xi_{i_1}(\omega), \ldots, \xi_{i_n}(\omega)) + \cdots, \tag{5}$$

where $I_n(\xi_{i_1}(\omega),\ldots,\xi_{i_n}(\omega))$ denote the Wiener–Askey polynomial chaos of order n in terms of ξ and N is defined in Remark 2. For notational convenience, Eq. (5) can be rewritten as

$$X(\omega) = \sum_{j=0}^{\infty} \hat{a}_j \psi_j(\boldsymbol{\xi}), \tag{6}$$

where the equality is interpreted in the $L_2(\Omega)$ sense and there is a one-to-one correspondence between $I_n(\xi_{i_1}(\omega),\ldots,\xi_{i_n}(\omega))$ and $\psi_j(\boldsymbol{\xi})$. Additionally, the following orthogonality relation holds:

$$\mathbb{E}\big(\psi_i(\boldsymbol{\xi})\psi_j(\boldsymbol{\xi})\big) := \int_{\mathbb{B}} \psi_i(\boldsymbol{\xi})\psi_j(\boldsymbol{\xi}) f(\boldsymbol{\xi})\, \mathrm{d}\boldsymbol{\xi} = \mathbb{E}\Big(\psi_i(\boldsymbol{\xi})^2\Big)\delta_{ij}, \tag{7}$$

where δ_{ij} is the Kronecker delta function and $f(\boldsymbol{\xi})$ is the joint PDF of $\boldsymbol{\xi}$. Karniadakis and co-workers [4] found that by choosing Askey polynomials with weighting function having same functional form as the joint PDF of $\boldsymbol{\xi}$, the GPCE Eq. (5) converges exponentially.

Remark 3. The GPCE encompasses the original polynomial chaos/Wiener–Hermite representation [17]. The convergence results proved by Cameron and Martin [18] for the original polynomial chaos, however, are not yet extended for the case of GPCE, which is motivated and supported solely by numerical experiments. Also, Eq. (6) is further truncated for computational purposes.

Pitfalls in the GPCE: From Eq. (5), the GPCE can be viewed as a Fourier-like expansion of $X(\omega)$ in terms of hypergeometric Askey polynomials in the random vector $\boldsymbol{\xi}$. Thus, if $X(\omega)$ as a function of ω possesses steep gradients or finite discontinuities, the GPCE approximation contains spurious oscillations (*Gibb's effect*). This invalidates the use of GPCE for addressing Problem II, wherein, the input–output uncertainty propagation is highly non-linear. In this paper, we propose the support space method to address the above (a localized representation of the output uncertainty along the lines of the stochastic Galerkin method [9]).

2.3. Support space representation of uncertainty

Let the inputs to a stochastic system be approximated using KLE with an input dimensionality N. This means that the stochastic inputs are represented in terms of N independent standard random variables $\xi_1(\omega),\ldots,\xi_N(\omega)$. If the PDF of $\xi_i(\omega)$ is given by a bounded function $f_{\xi_i}(\xi_i)$, then the joint PDF of inputs is given by

$$f(\boldsymbol{\xi}) = \prod_{i=1}^{N} f_{\xi_i}(\xi_i). \tag{8}$$

We can now define the input support space as follows:

$$A := \{\boldsymbol{\xi} := (\xi_1,\ldots,\xi_N) : f_{\xi_i}(\xi_i) > 0, \quad \text{for } i = 1,\ldots,N\}. \tag{9}$$

Using the Doob–Dynkin lemma [9], any solution $W(\mathbf{x},t,\omega)$ of the stochastic system can be represented as a function of inputs $\hat{W}(\mathbf{x},t,\boldsymbol{\xi})$. Now consider a discretization of the support space into disjoint finite element subdomains $A = \cup_{e=1}^{\mathrm{Nel}} A^{(e)}$ with a mesh size h (defined as the maximum diameter of $A^{(e)}$). The support-space representation of $W(\mathbf{x},t,\omega)$ (denoted as $W^h(\mathbf{x},t,\omega)$) is constructed as a piecewise polynomial of degree q in each element $A^{(e)}$. Note that the error in approximation of $W(\mathbf{x},t,\omega)$ behaves as follows:

$$\|W^h(\mathbf{x},t,\omega) - W(\mathbf{x},t,\omega)\|_{L_2(\Omega)} \leqslant \left(M\int_A \left(\hat{W}^h(\mathbf{x},t,\boldsymbol{\xi}) - \hat{W}(\mathbf{x},t,\boldsymbol{\xi})\right)^2 \mathrm{d}\boldsymbol{\xi}\right)^{\frac{1}{2}} \leqslant M^{\frac{1}{2}} C(\mathbf{x},t) h^{q+1}, \tag{10}$$

where $M = \max_{\xi \in A} f(\xi)$, $C(\mathbf{x}, t)$ is some deterministic function of space and time whose value depends on the nature of $W(\mathbf{x}, t, \omega)$ and q is the order of interpolation. We emphasize that the support-space representation includes GPCE as a special case when the number of elements is unity and the interpolating functions are Askey polynomials. In general, however, the convergence rate of the support space method is lower than that of GPCE and the method should not be used for modelling stochastic systems away from critical equilibrium points.

Remark 4. It can be shown that the LHS of Eq. (10) is penalized severely in the regions with large values for the input joint PDF $f(\xi)$. Hence, for computational purposes, we use an importance sampled gridding approach wherein the mesh discretization is refined at the high input PDF regions. Our initial investigations point that ISG increases numerical accuracy for the same discretization level.

Comparison between support-space and Wiener–Haar approach: Haar-wavelets necessarily constitute a piecewise constant representation/orthogonal sampling of a stochastic process whereas support-space is a finite element representation of a stochastic process. Wiener–Haar and the GPCE approaches complement each other (one can handle discontinuity in a more robust manner than the other), whereas, the support-space method is actually a super-set of the GPCE approach. This could imply that it is theoretically possible to attain the exponential convergence properties of the GPCE approach using the support-space approach (though more research is needed on this). This however is not true for the Wiener–Haar approach.

3. Problem definition

Consider a closed spatial region $\mathscr{D}$ with a piecewise smooth boundary Γ in the d-dimensional Euclidean space $\mathbb{R}^d$. Consider two different partitions of the boundary Γ denoted as $\Gamma_{gm} \cup \Gamma_{hm}$ and $\Gamma_{gt} \cup \Gamma_{ht}$, respectively, where $\Gamma_{gm} \cap \Gamma_{hm} = \emptyset$ and $\Gamma_{gm} \cap \Gamma_{hm} = \emptyset$. The system of equations governing natural convection of a Newtonian fluid under Boussinesq approximation can be written as follows. Find the non-dimensional stochastic velocity $\boldsymbol{v}(\mathbf{x}, t, \omega)$, stochastic pressure $p(\mathbf{x}, t, \omega)$ and stochastic temperature $\theta(\mathbf{x}, t, \omega)$ satisfying:

$$\frac{\partial \boldsymbol{v}}{\partial t} + \boldsymbol{v} \cdot \nabla \boldsymbol{v} = -Ra(\omega) Pr(\omega) \theta \boldsymbol{e}_g + \nabla \cdot \boldsymbol{\sigma}, \tag{11}$$

$$\nabla \cdot \boldsymbol{v} = 0, \tag{12}$$

$$\frac{\partial \theta}{\partial t} + \boldsymbol{v} \cdot \nabla \theta = \nabla^2 \theta, \tag{13}$$

$$\boldsymbol{v}(\mathbf{x}, t, \omega) = \boldsymbol{v}_g(\mathbf{x}, \omega), \quad (\mathbf{x}, t, \omega) \in \Gamma_{gm} \times \mathscr{T} \times \Omega, \tag{14}$$

$$\boldsymbol{n} \cdot \boldsymbol{\sigma}(\mathbf{x}, t, \omega) = \boldsymbol{h}(\mathbf{x}, \omega), \quad (\mathbf{x}, t, \omega) \in \Gamma_{hm} \times \mathscr{T} \times \Omega, \tag{15}$$

$$\boldsymbol{v}(\mathbf{x}, 0, \omega) = \boldsymbol{v}_0(\mathbf{x}, \omega), \quad (\mathbf{x}, t, \omega) \in \mathscr{D} \times \{0\} \times \Omega, \tag{16}$$

$$\theta(\mathbf{x}, t, \omega) = \theta_g(\mathbf{x}, \omega), \quad (\mathbf{x}, t, \omega) \in \Gamma_{gt} \times \mathscr{T} \times \Omega, \tag{17}$$

$$\nabla \theta(\mathbf{x}, t, \omega) \cdot \boldsymbol{n} = q_0(\mathbf{x}, \omega), \quad (\mathbf{x}, t, \omega) \in \Gamma_{ht} \times \mathscr{T} \times \Omega, \tag{18}$$

$$\theta(\mathbf{x}, 0, \omega) = \theta_0(\mathbf{x}, \omega), \quad (\mathbf{x}, t, \omega) \in \mathscr{D} \times \{0\} \times \Omega, \tag{19}$$

where $\boldsymbol{\sigma}$ is defined as $-p\boldsymbol{I} + 2Pr(\omega)\boldsymbol{\epsilon}(\boldsymbol{v})$ and $\boldsymbol{\epsilon}(\boldsymbol{v})$ is defined as $[(\nabla \boldsymbol{v}) + (\nabla \boldsymbol{v})^{\mathrm{T}}]/2$. The stochastic non-dimensional parameters $Ra(\omega)$ and $Pr(\omega)$ denote the Rayleigh number and the Prandtl number, respectively

(defined later for each numerical example in Section 6). These parameters completely govern the evolution of the natural convection system. In fact, CP1 corresponds to a critical Rayleigh number Ra_c.

We will now apply the variational multiscale method (VMS) to derive a stabilized finite element formulation for the solution of Eqs. (11)–(19).

4. Variational multiscale method

Consider the following function spaces:

$$\mathscr{V} = \left\{ \boldsymbol{v} : \boldsymbol{v} \in [L_2(\Omega; L_2(\mathscr{T}; H^1(\mathscr{D})))]^d, \quad \boldsymbol{v} = \boldsymbol{v}_g \text{ on } \Gamma_{gm} \right\}, \tag{20}$$

$$\mathscr{V}_0 = \left\{ \boldsymbol{w} : \boldsymbol{w} \in \left[L_2(\Omega; H^1(\mathscr{D}))\right]^d, \quad \boldsymbol{w} = \boldsymbol{0} \text{ on } \Gamma_{gm} \right\}, \tag{21}$$

$$\mathscr{Q} = \{ p : p \in L_2(\Omega; L_1(\mathscr{T}; L_2(\mathscr{D}))) \}, \tag{22}$$

$$\mathscr{Q}_0 = \{ q : q \in L_2(\Omega; L_2(\mathscr{D})) \}, \tag{23}$$

$$\mathscr{E} = \left\{ \theta : \theta \in L_2(\Omega; L_2(\mathscr{T}; H^1(\mathscr{D}))), \quad \theta = \theta_g \text{ on } \Gamma_{gt} \right\}, \tag{24}$$

$$\mathscr{E}_0 = \left\{ w : w \in L_2(\Omega; H^1(\mathscr{D})), \quad w = 0 \text{ on } \Gamma_{gt} \right\}. \tag{25}$$

Remark 5. The model Eqs. (11)–(13) form a system of coupled SPDEs. Hence, their solution requires a non-linear iterative approach. Here, we will consider the non-dimensional stochastic velocity to be known when solving for the non-dimensional temperature and vice-versa. We will also denote the known velocity as $\mathbf{a}(\mathbf{x}, \omega)$, a spatially varying divergence-free stochastic velocity field that is usually taken as the previous non-linear iteration solution.

Variational formulation for energy conservation equation: Find the non-dimensional stochastic temperature $\theta \in \mathscr{E}$ such that for all $w \in \mathscr{E}_0$ the following relation holds:

$$(\partial_t \theta, w) + (\mathbf{a} \cdot \nabla \theta, w) + (\nabla \theta, \nabla w)_v = (q_0, w)_{\Gamma_{ht}}, \tag{26}$$

where the bilinear quantities are defined as follows:

$$(g, h) := \int_\Omega \int_{\mathscr{D}} gh \, \mathrm{d}\mathbf{x} \, \mathrm{d}\mathscr{P}, \quad (g, h)_v := \int_\Omega \int_{\mathscr{D}} g \cdot h \, \mathrm{d}\mathbf{x} \, \mathrm{d}\mathscr{P}. \tag{27}$$

Variational formulation for mass and momentum conservation equations: Find the non-dimensional stochastic velocity and pressure $[\boldsymbol{v}, p] \in \mathscr{V} \times \mathscr{Q}$ such that for all $[\mathbf{w}, q] \in \mathscr{V}_0 \times \mathscr{Q}_0$, the following relations hold:

$$(\partial_t \boldsymbol{v}, \boldsymbol{w}) + (\boldsymbol{v} \cdot \nabla \boldsymbol{v}, \boldsymbol{w}) + (\boldsymbol{\sigma}, \boldsymbol{\epsilon}(\boldsymbol{w}))_v = -(Ra(\omega) Pr(\omega) \theta \boldsymbol{e}_g, \boldsymbol{w}) + (\boldsymbol{h}, \boldsymbol{w})_{\Gamma_{hm}}, \tag{28}$$

$$(\nabla \cdot \boldsymbol{v}, q) = 0, \tag{29}$$

where the bilinear quantities are defined as follows:

$$(\mathbf{g}, \boldsymbol{h}) := \int_\Omega \int_{\mathscr{D}} \mathbf{g} \cdot \mathbf{h} \, \mathrm{d}\mathbf{x} \, \mathrm{d}\mathscr{P}, \quad (\mathbf{g}, \boldsymbol{h})_v := \int_\Omega \int_{\mathscr{D}} \mathbf{g} : \mathbf{h} \, \mathrm{d}\mathbf{x} \, \mathrm{d}\mathscr{P}. \tag{30}$$

It is well documented that the use of standard Galerkin finite elements for the solution of Eqs. (26)–(29) leads to spurious oscillations in the solution [11]. Thus, we require a stabilized finite element approach. We will use the VMS approach for the derivation of a stabilized finite element formulation.

Additive scale decomposition: Under the VMS approach, we consider an additive scale decomposition for the non-dimensional stochastic velocity, pressure and temperature of the form $\boldsymbol{v} = \bar{\boldsymbol{v}} + \boldsymbol{v}', p = \bar{p} + p'$ and $\theta = \bar{\theta} + \theta'$; where the quantities with a bar indicate the large scale solution contributions that can be resolved by the computational grid and the quantities with a prime indicate the subgrid scale solutions that denote the unresolved solution components. This decomposition of solutions induces a similar decomposition for the corresponding function spaces as $\mathscr{V} = \bar{\mathscr{V}} \oplus \mathscr{V}', \mathscr{V}_0 = \bar{\mathscr{V}}_0 \oplus \mathscr{V}'_0, \mathscr{Q} = \bar{\mathscr{Q}} \oplus \mathscr{Q}', \mathscr{Q}_0 = \bar{\mathscr{Q}}_0 \oplus \mathscr{Q}'_0, \mathscr{E} = \bar{\mathscr{E}} \oplus \mathscr{E}'$ and $\mathscr{E}_0 = \bar{\mathscr{E}}_0 \oplus \mathscr{E}'_0$.

4.1. Scale decomposed variational formulation for energy equation

By introducing the variational multiscale decomposition for temperature, we obtain the following large scale and subgrid scale variational equations:

$$(\partial_t \bar{\theta} + \partial_t \theta', \bar{w}) + (\mathbf{a} \cdot \nabla \bar{\theta} + \mathbf{a} \cdot \nabla \theta', \bar{w}) + (\nabla \bar{\theta} + \nabla \theta', \nabla \bar{w})_v = (q_0, \bar{w})_{\Gamma_{ht}}, \tag{31}$$

$$(\partial_t \bar{\theta} + \partial_t \theta', w') + (\mathbf{a} \cdot \nabla \bar{\theta} + \mathbf{a} \cdot \nabla \theta', w') + (\nabla \bar{\theta} + \nabla \theta', \nabla w')_v = (q_0, w')_{\Gamma_{ht}}. \tag{32}$$

With imposed condition of a twice-differentiable subgrid scale solution, we can express Eq. (32) in its strong form as follows:

$$\partial_t \theta' + \mathbf{a} \cdot \nabla \theta' - \nabla^2 \theta' = -(\partial_t \bar{\theta} + \mathbf{a} \cdot \nabla \bar{\theta} - \nabla^2 \bar{\theta}), \tag{33}$$

where the RHS of the above equation is to be understood in the sense that it represents the projection of large scale residual of the energy equation onto the small scale function space $\mathscr{E}'$.

Without loss of generality, we shall now consider a one-step trapezoidal rule for time integration. Consider the following notations for a generic quantity f:

$$\partial_t f_n = \frac{1}{\delta t}(f_{n+1} - f_n), \quad f_{n+\gamma} = \gamma f_{n+1} + (1-\gamma) f_n, \tag{34}$$

where f_{n+1} and f_n denote the values of f at time levels n and $(n+1)$, respectively and γ is a parameter between zero and one (taken as 0.5 in all numerical examples in Section 6).

After applying the time discretization to θ, we can rewrite Eq. (33) as follows:

$$\partial_t \theta'_n + \mathscr{L} \theta'_{n+\gamma} = R_{n+\gamma}, \tag{35}$$

where the operator $\mathscr{L}$ and the residual $R_{n+\gamma}$ are defined as follows:

$$\mathscr{L} := \mathbf{a} \cdot \nabla - \nabla^2, \quad R_{n+\gamma} := -\partial_t \bar{\theta}_n - \mathbf{a} \cdot \nabla \bar{\theta}_{n+\gamma} + \nabla^2 \bar{\theta}_{n+\gamma}. \tag{36}$$

Derivation of algebraic subgrid scale solution model: We shall now proceed in the derivation along the lines of [10,19,20]. Consider a finite element discretization of the domain $\mathscr{D}$ into a number of disjoint element subdomains $\mathscr{D}^{(e)} : e = 1, \ldots, \mathrm{Nel}$; where Nel is the number of element subdomains. By taking the element-wise Fourier transform of Eq. (35), we obtain:

$$\left(\frac{1}{\gamma \delta t} + \mathbf{i} \frac{\mathbf{a} \cdot \mathbf{k}}{h} + \frac{|\mathbf{k}|^2}{h^2} \right) \hat{\theta}'_{n+\gamma} = \hat{R}_{n+\gamma} + \frac{1}{\gamma \delta t} \hat{\theta}'_n. \tag{37}$$

Now, by application of Plancheral's formula and mean value theorem, we end up with the following approximate algebraic stochastic subgrid scale solution model for $\theta'_{n+\gamma}$:

$$\theta'_{n+\gamma} \overset{L_2}{\approx} \tau_t \left(R_{n+\gamma} + \frac{1}{\gamma \delta t} \theta'_n \right), \quad \tau_t := \left(\left(c_1 \frac{1}{h^2} + \frac{1}{\gamma \delta t} \right)^2 + \left(c_2 \frac{|\mathbf{a}|}{h} \right)^2 \right)^{-\frac{1}{2}}. \tag{38}$$

The approximation in Eq. (38) is to be interpreted in the L_2-sense and the parameters c_1 and c_2 are model constants. The stabilization parameter τ_t is also called as the stochastic intrinsic subgrid time scale for the energy equation.

Remark 6. The stabilization parameter in Eq. (38) differs from that in [10] due to the presence of a time-step parameter δt. Nevertheless, the asymptotic behavior of the parameters remains unaltered. Also, the subgrid model has the subgrid solution at previous time level in the RHS. This term does not arise if we assume a quasi-static subgrid solution.

VMS stabilized formulation: With strong regularity conditions (twice-differentiable temperature) we obtain

$$(\mathbf{a} \cdot \nabla \theta'_{n+\gamma}, \bar{w}) = -(\theta'_{n+\gamma}, \mathbf{a} \cdot \nabla \bar{w}), \quad (\nabla \theta'_{n+\gamma}, \nabla \bar{w})_v = -(\theta'_{n+\gamma}, \nabla^2 \bar{w}). \tag{39}$$

We can now combine Eqs. (31), (38) and (39) to obtain a stabilized formulation as follows:

$$\begin{aligned} &(\partial_t \bar{\theta}_n, \bar{w}) + (\mathbf{a} \cdot \nabla \bar{\theta}_{n+\gamma}, \bar{w}) + (\nabla \bar{\theta}_{n+\gamma}, \nabla \bar{w})_v - (\bar{q}_0, \bar{w})_{\Gamma_{ht}} + \mathop{\mathsf{A}}_{e=1}^{\mathrm{Nel}} \big[(\partial_t \bar{\theta}_n + \mathbf{a} \cdot \nabla \bar{\theta}_{n+\gamma} - \nabla^2 \bar{\theta}_{n+\gamma}, -\tau_t \tilde{w} \\ &\quad + \tau_t \mathbf{a} \cdot \nabla \bar{w} + \tau_t \nabla^2 \bar{w}) + (\theta'_n, \tau_t \tilde{w}/(\gamma \delta t) - \tau_t \mathbf{a} \cdot \nabla \tilde{w} - \tau_t \nabla^2 \tilde{w} - \tilde{w}) \big] = 0, \end{aligned} \tag{40}$$

where the terms under square brackets are element-wise integrals and other remaining terms are domain integrals. Also, $\tilde{w}$ is defined as $\bar{w}/(\gamma \delta t)$. Numerical tests show that the effect of subgrid tracking on stabilization is extremely small for laminar flow regime and hence, a quasi-static subgrid scale assumption $\partial_t \theta' \approx 0$ can help in reducing the computational and memory cost.

4.2. Scale decomposed variational formulation for mass and momentum conservation equations

By introducing the variational multiscale decomposition for velocity and pressure, we obtain the following large scale and subgrid scale variational equations:

$$\begin{aligned} &(\partial_t \bar{\boldsymbol{v}} + \partial_t \boldsymbol{v}', \bar{\boldsymbol{w}}) + (\mathbf{a} \cdot \nabla \bar{\boldsymbol{v}} + \mathbf{a} \cdot \nabla \boldsymbol{v}', \bar{\boldsymbol{w}}) + (\boldsymbol{\sigma}(\bar{\boldsymbol{v}}, \bar{p}), \boldsymbol{\epsilon}(\bar{\boldsymbol{w}}))_v + (\boldsymbol{\sigma}(\boldsymbol{v}', p'), \boldsymbol{\epsilon}(\bar{\boldsymbol{w}}))_v \\ &\quad + (Ra(\omega) Pr(\omega) \theta \boldsymbol{e}_g, \bar{\boldsymbol{w}}) - (\boldsymbol{h}, \bar{\boldsymbol{w}})_{\Gamma_{hm}} = 0, \end{aligned} \tag{41}$$

$$(\nabla \cdot \bar{\boldsymbol{v}}, \bar{q}) = 0, \tag{42}$$

$$\begin{aligned} &(\partial_t \bar{\boldsymbol{v}} + \partial_t \boldsymbol{v}', \boldsymbol{w}') + (\mathbf{a} \cdot \nabla \bar{\boldsymbol{v}} + \mathbf{a} \cdot \nabla \boldsymbol{v}', \boldsymbol{w}') + (\boldsymbol{\sigma}(\bar{\boldsymbol{v}}, \bar{p}), \boldsymbol{\epsilon}(\boldsymbol{w}'))_v + (\boldsymbol{\sigma}(\boldsymbol{v}', p'), \boldsymbol{\epsilon}(\boldsymbol{w}'))_v \\ &\quad + (Ra(\omega) Pr(\omega) \theta \boldsymbol{e}_g, \boldsymbol{w}') + (\boldsymbol{h}, \boldsymbol{w}')_{\Gamma_{hm}} = 0, \end{aligned} \tag{43}$$

$$(\nabla \cdot \bar{\boldsymbol{v}}, q') = 0. \tag{44}$$

We use Picard's linearization approach for the non-linear convection term $\boldsymbol{v} \cdot \nabla \boldsymbol{v} \approx \mathbf{a} \cdot \nabla \bar{\mathbf{v}} + \mathbf{a} \cdot \nabla \boldsymbol{v}'$, where $\mathbf{a}$ is defined in Remark 5. Now, by assuming a twice-differentiable subgrid scale solution (velocity and pressure), we can express Eqs. (43) and (44) in their strong forms as follows:

$$\partial_t \boldsymbol{v}' + \mathbf{a} \cdot \nabla \mathbf{v}' - \nabla \cdot \boldsymbol{\sigma}(\mathbf{v}', p') = -Ra(\omega) Pr(\omega) \theta \boldsymbol{e}_g - \partial_t \bar{\mathbf{v}} - \mathbf{a} \cdot \nabla \bar{\boldsymbol{v}} + \nabla \cdot \boldsymbol{\sigma}(\bar{\mathbf{v}}, \bar{p}), \tag{45}$$

$$\nabla \cdot \boldsymbol{v}' = -\nabla \cdot \bar{\boldsymbol{v}}, \tag{46}$$

where the RHS of the above equations is to be understood as the projection of large scale residual of the energy and continuity equation onto the small scale function space $\mathscr{V}' \times \mathscr{Q}'$. By carrying out an analysis similar to the energy equation, we arrive at the following subgrid scale models:

$$p'_{n+\gamma} = \tau_{(c)} R_c, \quad \tau_{(c)} = \left(\left(\frac{h^2}{c_1 \gamma \delta t} + Pr(\omega) \right)^2 + \left(\frac{c_2 |\mathbf{a}| h}{c_1} \right) \right)^{\frac{1}{2}}, \tag{47}$$

$$\mathbf{v}'_{n+\gamma} = \tau_{(m)} \left(R_m + \frac{\mathbf{v}'_n}{\gamma \delta t} \right), \quad \tau_{(m)} = \frac{h^2}{c_1 \tau_{(c)}}, \tag{48}$$

where c_1 and c_2 have the same interpretation as for the energy equation.

VMS stabilized formulation: With strong regularity conditions (twice-differentiable velocity and once continuously differentiable pressure), we obtain the following:

$$\begin{aligned} &(\mathbf{a} \cdot \nabla \mathbf{v}'_{n+\gamma}, \bar{\mathbf{w}}) = -(\mathbf{v}'_{n+\gamma}, \mathbf{a} \cdot \nabla \bar{\mathbf{w}}), \\ &(Pr(\omega) \boldsymbol{\epsilon}(\mathbf{v}'_{n+\gamma}), \boldsymbol{\epsilon}(\bar{\mathbf{w}}))_v = -(\mathbf{v}'_{n+\gamma}, Pr(\omega) \nabla \cdot \boldsymbol{\epsilon}(\bar{\mathbf{w}})). \end{aligned} \tag{49}$$

We can combine Eqs. (41), (42) and (47)–(49) to obtain the following stabilized formulation for momentum and mass conservation equations:

$$\begin{aligned} &(\partial_t \bar{\mathbf{v}}_n + \mathbf{a} \cdot \nabla \bar{\mathbf{v}}_{n+\gamma}, \bar{\mathbf{w}}) - (\boldsymbol{\sigma}(\bar{\mathbf{v}}_{n+\gamma}, \bar{p}_{n+\gamma}), \boldsymbol{\epsilon}(\bar{\mathbf{w}}))_v + (Ra(\omega) Pr(\omega) \theta \mathbf{e}_g, \bar{\mathbf{w}}) \\ &\quad + \mathop{\mathsf{A}}_{e=1}^{\mathrm{Nel}} \big[\big(Ra(\omega) Pr(\omega) \theta \mathbf{e}_g + \partial_t \bar{\mathbf{v}}_n + \mathbf{a} \cdot \nabla \bar{\mathbf{v}}_{n+\gamma} - \nabla \cdot \boldsymbol{\sigma}(\bar{\mathbf{v}}_{n+\gamma}, \bar{p}_{n+\gamma}) \\ &\quad - \mathbf{v}'_n / (\gamma \delta t), -\tau_{(m)} (\tilde{\mathbf{w}} + \mathbf{a} \cdot \nabla \bar{\mathbf{w}} + Pr(\omega) \nabla \cdot \boldsymbol{\epsilon}(\bar{\mathbf{w}})) \big) \big] - (\bar{\boldsymbol{h}}, \bar{\mathbf{w}})_{\Gamma_{hm}} = 0, \end{aligned} \tag{50}$$

$$(\nabla \cdot \bar{\mathbf{v}}_{n+\gamma}, \bar{q}) + \mathop{\mathsf{A}}_{e=1}^{\mathrm{Nel}} \big[\big(Ra(\omega) Pr(\omega) \theta \mathbf{e}_g + \partial_t \bar{\mathbf{v}}_n + \mathbf{a} \cdot \nabla \bar{\mathbf{v}}_{n+\gamma} - \nabla \cdot \boldsymbol{\sigma}(\bar{\mathbf{v}}_{n+\gamma}, \bar{p}_{n+\gamma}) - \mathbf{v}'_n / (\gamma \delta t), \tau_{(m)} \nabla \bar{q} \big) \big] = 0, \tag{51}$$

where the terms in square brackets are element-wise integrals and all other terms are whole domain integrals. Also, $\tilde{\mathbf{w}}$ is defined as $\bar{\mathbf{w}}/(\gamma \delta t)$. We can observe that the subgrid scale solution at the previous time step and the time step size play a role in stabilizing the finite element formulation.

5. Algorithm and finite element implementation details

5.1. Implementation of the generalized polynomial chaos approach

Let the spatial domain be divided into Nel finite element subdomains and the number of basis functions in each element equals nbf. We can represent a generic large scale stochastic function $\bar{f}(\mathbf{x}, \omega)$ in its GPCE as follows:

$$\bar{f}(\mathbf{x}, \omega) = \sum_{j=0}^{P} \bar{f}_j(\mathbf{x}) \psi_j(\omega), \tag{52}$$

Note that here we choose to truncate the series expansion in Eq. (6) to the first $(P + 1)$ terms. We now represent each function $\bar{f}_j(\mathbf{x})$ in a piecewise polynomial finite element representation

$$\bar{f}(\mathbf{x},\omega) = \sum_{j=0}^{P} \sum_{\alpha=1}^{\mathrm{nbf}} \bar{f}_{\alpha j} N_\alpha(\mathbf{x}) \psi_j(\omega). \tag{53}$$

This can be written as

$$\bar{f}(\mathbf{x},\omega) = \sum_{r=0}^{\mathrm{nbf}(P+1)-1} W_r(\mathbf{x},\omega) \bar{f}_r, \tag{54}$$

where $r = (\alpha - 1)(P + 1) + j$ with $\alpha = 1, \ldots \mathrm{nbf}$, $j = 0, \ldots, P$, and the stochastic finite element weighting functions are now interpreted as the product of a standard Galerkin shape function with a generalized polynomial chaos. The storage of the large scale solution and the subgrid solution requires a $\mathrm{ndof} \times (P + 1)$ and a $\mathrm{Nel} \times \mathrm{nbf}$ array, respectively, where ndof denotes the number of degrees of freedom.

5.2. Implementation of a support-space/stochastic Galerkin finite element approach

Here, we use a dual-layered grid. In the top layer, the spatial grid comprises of Nel elements, each with nInt integration points and nbf basis functions. At each integration point, the spatial grid has a pointer to an underlying support-space grid. We discretize the support-space grid using the importance sampled gridding approach (refining the grid in regions with high input joint PDF). The support-space grid comprises of $\mathrm{Nel}^{\mathrm{s}}$ element subdomains such that $\mathscr{A} = \cup_{e^{\mathrm{s}}=1}^{\mathrm{Nel}^{\mathrm{s}}} \mathscr{A}^{(e^{\mathrm{s}})}$. Each support-space grid element has $\mathrm{nbf}^{\mathrm{s}}$ basis functions. Any random large-scale function $\bar{f}(\mathbf{x},\omega)$ is now represented at any spatial location as follows:

$$\bar{f}(\mathbf{x},\omega) = \sum_{\alpha=1}^{\mathrm{nbf}} \bar{f}^h_\alpha(\omega) N_\alpha(\mathbf{x}), \tag{55}$$

where $\bar{f}^h_\alpha$ is a finite element field defined on the support-space grid. Further, the value of the large scale function at a given value of inputs $\boldsymbol{\xi}_{\mathrm{given}} \in \mathscr{A}^{(e^{\mathrm{s}})}$ is obtained as follows:

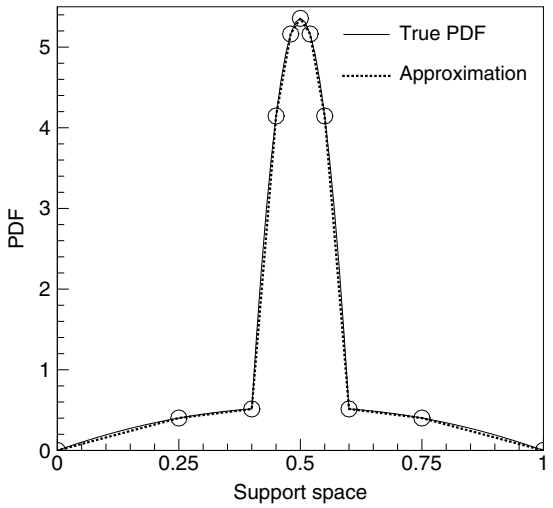

Fig. 1. Probability density function PDF of a single stochastic input (assumed), interpolant of the PDF and the support space grid. The circles denote the nodal points of the support space grid.

$$\bar{f}(\mathbf{x},\omega) = \sum_{\alpha=1}^{\mathrm{nbf}} \sum_{j=1}^{\mathrm{nbf^s}} \bar{f}_{j\alpha} N_j^{\mathrm{s}}(\boldsymbol{\xi}_{\mathrm{given}}) N_\alpha(\mathbf{x}). \tag{56}$$

Thus the storage of the large scale solution and subgrid scale solution requires a ndof × ndof$^{\mathrm{s}}$ and a Nel × nInt (per degree of freedom) array, respectively, where ndof and ndof$^{\mathrm{s}}$ denote the number of degrees of freedom for the spatial domain and the support-space grid, respectively.

Remark 7. The support-space grid is adaptively refined at points of relatively large input joint PDF. The actual probability density, the support-space grid and the approximation to the PDF for the case of a single stochastic input is given in Fig. 1. It can be observed that the maximum point of the PDF has a node. The discretization is refined proportional to the value of the PDF. This ensures that the error between the actual PDF and its interpolant is minimized in the mean square sense.

5.3. Details of the solution algorithm

- Step 1: At time $t = 0$, large scale temperature, velocity and pressure are assumed known (taken to be the initial conditions). The small scale solutions are taken to be zero.
- Step 2: For $n = 0, 1, 2, \ldots$, do the following steps:
  - Calculate $\theta'_{n-1}, \mathbf{v}'_{n-1}$ if n is not zero.
  - Solve for $\bar{\theta}_{n+\gamma}$ assuming known velocity $\bar{\boldsymbol{v}}$ and $\boldsymbol{v}'$. (These are the stochastic velocity solutions at previous non-linear iteration level.)
  - Solve for $\bar{\boldsymbol{v}}_{n+\gamma}$ assuming known temperature $\bar{\theta}$ and θ'. (These are the stochastic temperature solutions obtained from $\bar{\theta}_{n+\gamma}$ and θ' from previous non-linear iteration).
  - Using $\bar{\theta}_{n+\gamma}$, obtain an estimate of $\theta'_{n+\gamma}$ at each integration point within an element.
  - Using $\bar{\boldsymbol{v}}_{n+\gamma}$, obtain an estimate of $\mathbf{v}'_{n+\gamma}$ at each integration point within an element.
  - Compute the next time step quantities $\bar{\boldsymbol{v}}_{n+1}, \bar{p}_{n+1}$ and $\bar{\theta}_{n+1}$.
  - If the solution has converged, proceed. Else, iterate step 2.
- End of algorithm.

6. Numerical examples

In this section, we consider numerical examples based on the focus of this paper:

- Example I. *Simulation of natural convection away from critical equilibrium points (Problem I)*: Air at 293 K in a square cavity with an adiabatic body at the center.
- Example II. *Simulation of natural convection near CP1 (Problem II)*: Water at 293 K in a square cavity.

Notation: g, gravitational acceleration; β, coefficient of thermal expansion of the fluid; ν, kinematic viscosity of the fluid and α, diffusivity of the fluid.

The Rayleigh and Prandtl numbers in each example are defined as

$$Ra = \frac{g\beta L^3 \Delta T_{\mathrm{ref}}}{\nu\alpha}, \quad Pr = \frac{\nu}{\alpha},$$

where the characteristic length L and the reference temperature scale ΔT_{ref} are problem dependant and will be defined separately for each example.

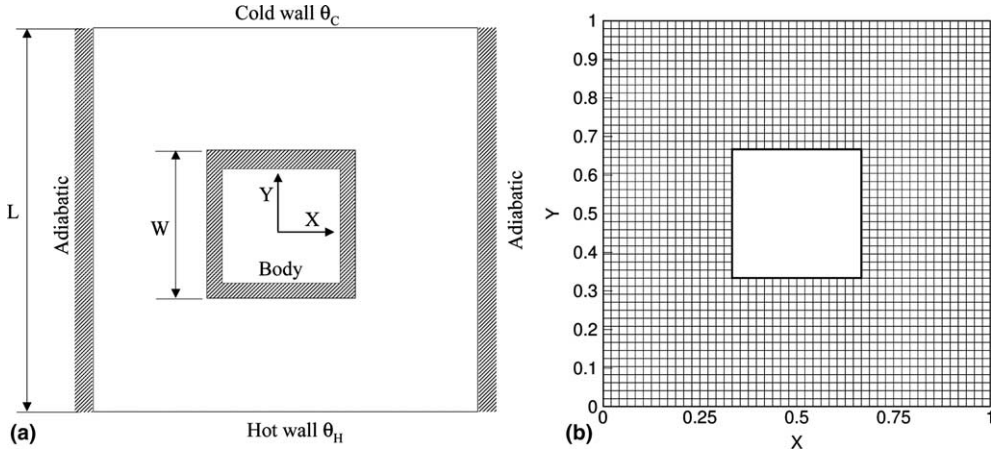

Fig. 2. Example I: (a) schematic of the computational domain; (b) mesh.

6.1. Example I

Consider a square enclosure with a square adiabatic body at the center (see Fig. 2(a)). The enclosure is filled with air at 293 K. The bottom wall of the enclosure is maintained at $T_H > 293$ K, where T_H is modelled as a uniform random variable. The dimensionless temperature $\theta_H = (T_H - 293\ \text{K})/(\mathbb{E}(T_H) - 293\ \text{K})$ is defined as follows:

$$\theta_H = 1.0 + 0.05\xi, \quad \xi \overset{\text{d}}{=} U[-1, 1],$$

where $\overset{\text{d}}{=}$ means 'is distributed as' and $U[a, b]$ denotes a uniform distribution in the interval between a and b. The side walls are assumed to be adiabatic and $\theta_C = 0$, $W = L/3$ (see Fig. 2(a)), the Prandtl number is 0.7

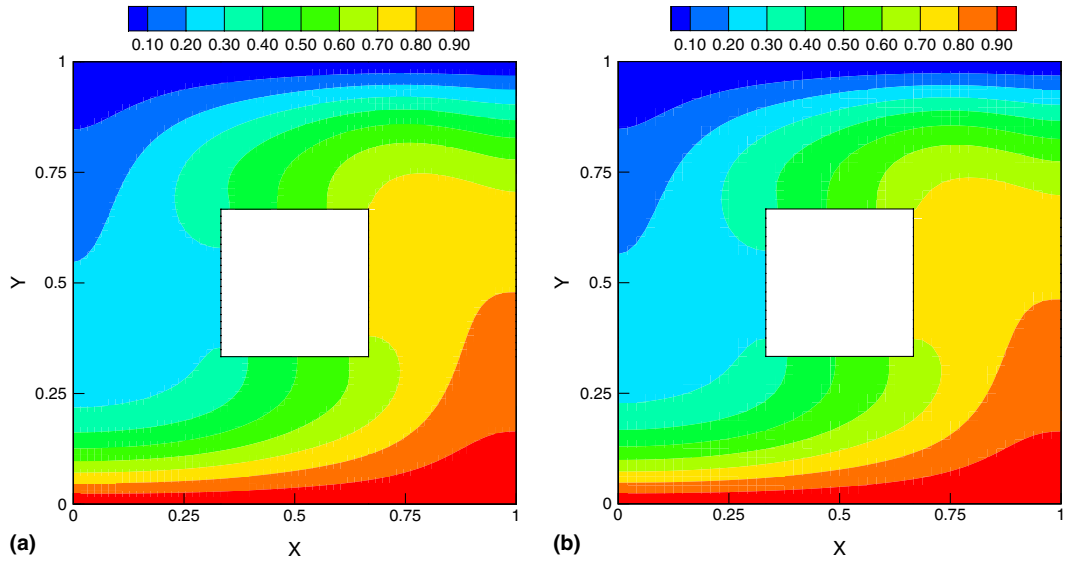

Fig. 3. Example I: (a) deterministic non-dimensional temperature at steady state; (b) mean non-dimensional temperature at steady state.

and the Rayleigh number based on the enclosure side-length L and the temperature scale $\mathbb{E}(T_H) - 293$ K is 10^4. Thus, Ra is considered to be a deterministic quantity and the randomness is incorporated in the hot wall boundary conditions. In Example II, we will consider an alternative approach. For this combination of input parameters, the above natural convection system is away from any critical points. Thus the dependance of output uncertainty on the input uncertainty is smooth. Hence, the GPCE approach yields an exponentially convergent approximation to the outputs.

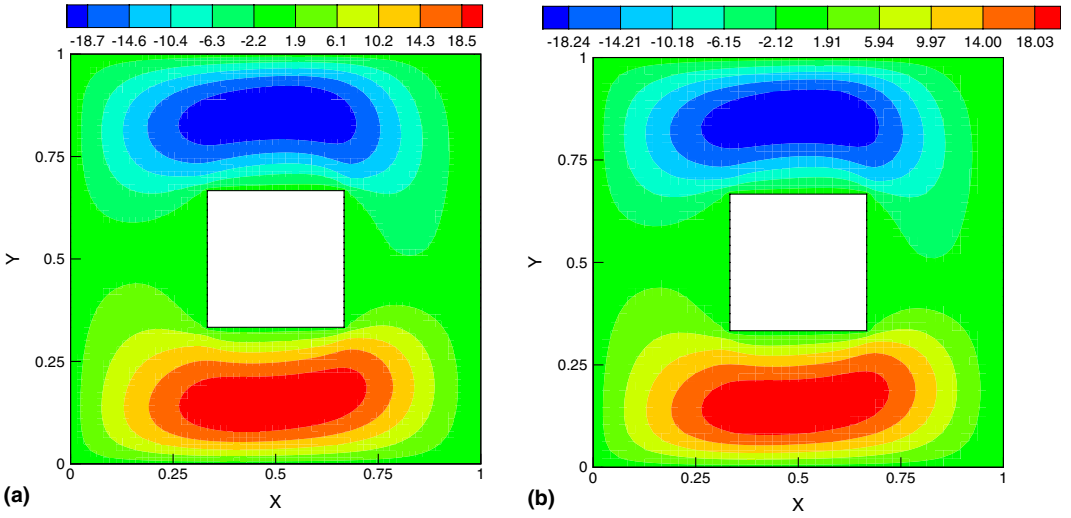

Fig. 4. Example I: (a) deterministic non-dimensional x-velocity component at steady state; (b) mean non-dimensional x-velocity component at steady state.

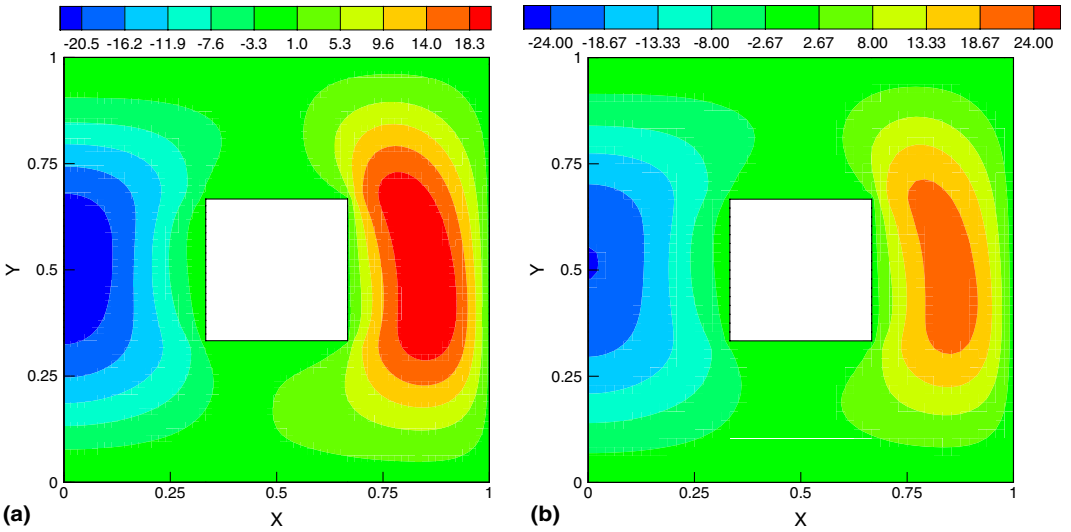

Fig. 5. Example I: (a) deterministic non-dimensional y-velocity component at steady state; (b) mean non-dimensional y-velocity component at steady state.

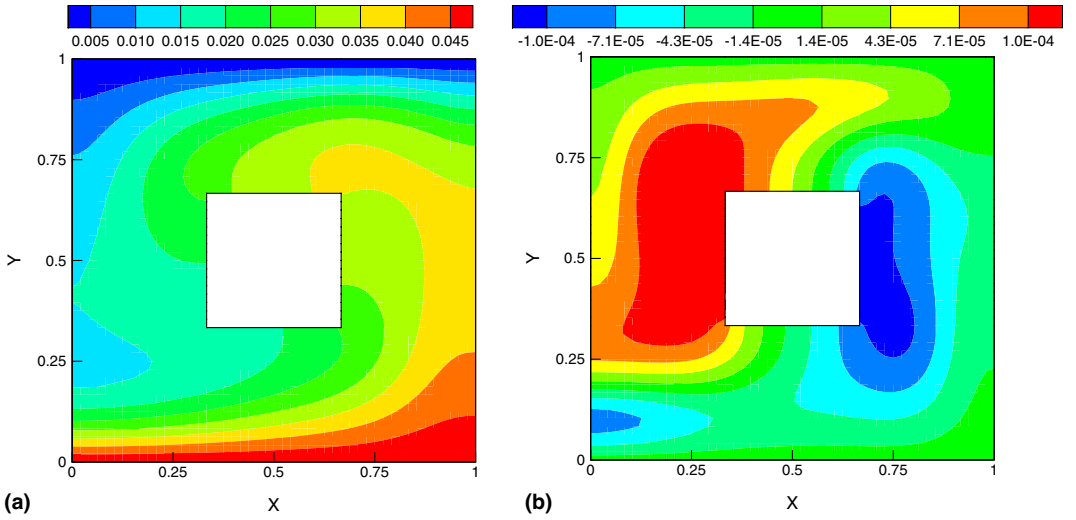

Fig. 6. Example I: (a) first-order term in Legendre chaos expansion of non-dimensional temperature at steady state; (b) second-order term in Legendre chaos expansion of non-dimensional temperature at steady state.

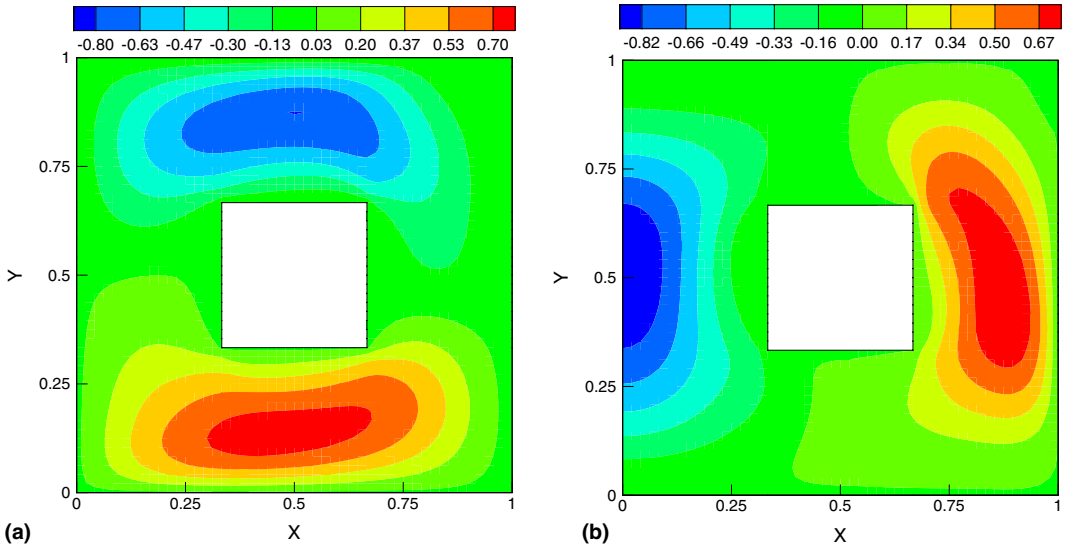

Fig. 7. Example I: (a) first-order term in Legendre chaos expansion of non-dimensional x-velocity component at steady state; (b) second-order term in Legendre chaos expansion of non-dimensional x-velocity component at steady state.

A schematic of the computational mesh used for spatial discretization of the problem is provided in Fig. 2(b). A deterministic simulation with $\theta_H = 1.0$, $Pr = 0.7$ and $Ra = 10^4$ is used to compare the results at steady state. A third-order Legendre chaos expansion (since input is uniformly distributed) was used for representation of the temperature and flow fields. Instead of proceeding toward a symmetric steady state about the centerlines of the square cavity as characterized by Rayleigh numbers less than 4×10^3 [21], we observe in Figs. 3–8 that the steady state (computed at $t = 1.5$) is characteristic of Rayleigh–Bénard convection without square body at the center. The mean temperature and velocity components correspond fairly well

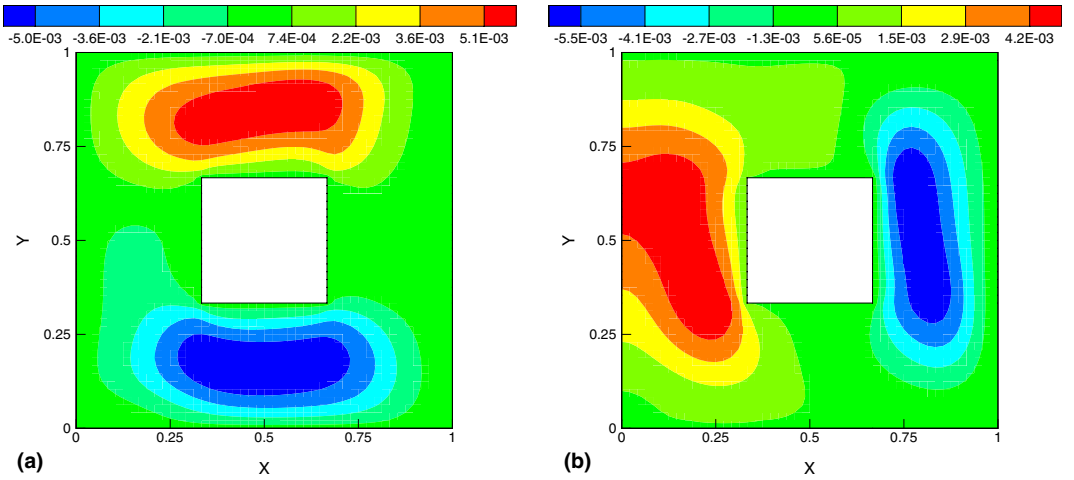

Fig. 8. Example I: (a) first-order term in Legendre chaos expansion of non-dimensional y-velocity component at steady state; (b) second-order term in Legendre chaos expansion of non-dimensional y-velocity component at steady state.

with the deterministic simulation results. Figs. 3(a) and (b) show the comparisons for steady-state temperature, Figs. 4(a) and (b) show the comparisons for the x-velocity component and Figs. 5(a) and (b) show the comparisons for the y-velocity component.

For the sake of completion, we also include the higher order coefficients of Legendre chaos corresponding to the steady-state temperature and velocity in Figs. 6–8.

6.2. Example II

Consider a closed square cavity filled with water at 293 K. The bottom wall of the cavity is maintained at an unknown temperature $T_H > 293$ K. The side walls are assumed to be adiabatic. The top wall is kept at a

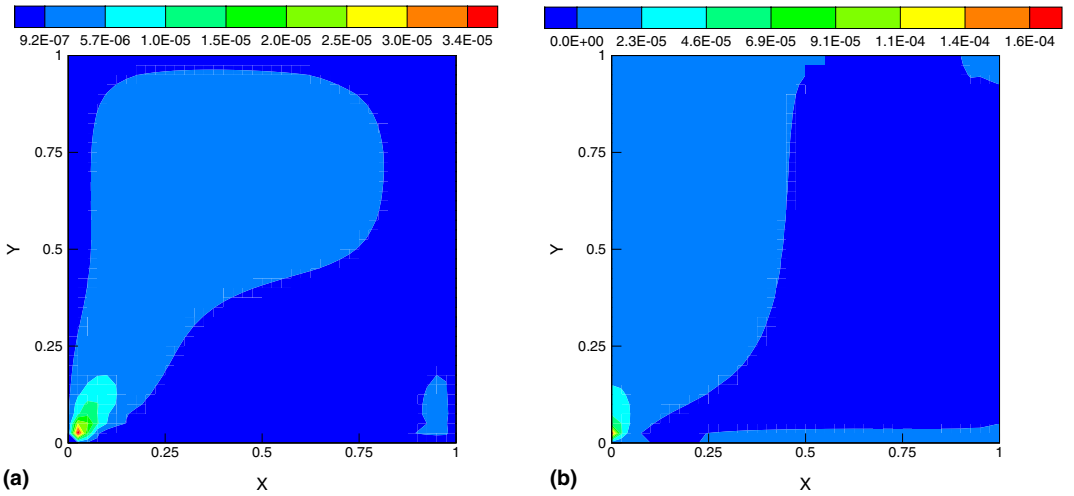

Fig. 9. Example II: (a) mean non-dimensional x-velocity component at steady state using GPCE approach; (b) mean non-dimensional y-velocity component at steady state using GPCE approach.

constant temperature of 293 K. The Prandtl number is 6.95 and the Rayleigh number Ra is defined using the side wall length and a stochastic temperature scale $T_H - 293$ K. Here, unlike Example I, the stochastic temperature scale induces a randomness in the Rayleigh number and the boundary conditions for the non-dimensional solutions are taken to be deterministic.

This system is characterized by the first critical point CP1 at a Rayleigh number of $Ra_c \approx 1700$. Below this Rayleigh number, the heat transfer is by conduction and the fluid flow is absent. Above Ra_c, well known Rayleigh–Bénard instabilities are initiated. By modelling the Rayleigh number as a uniform random

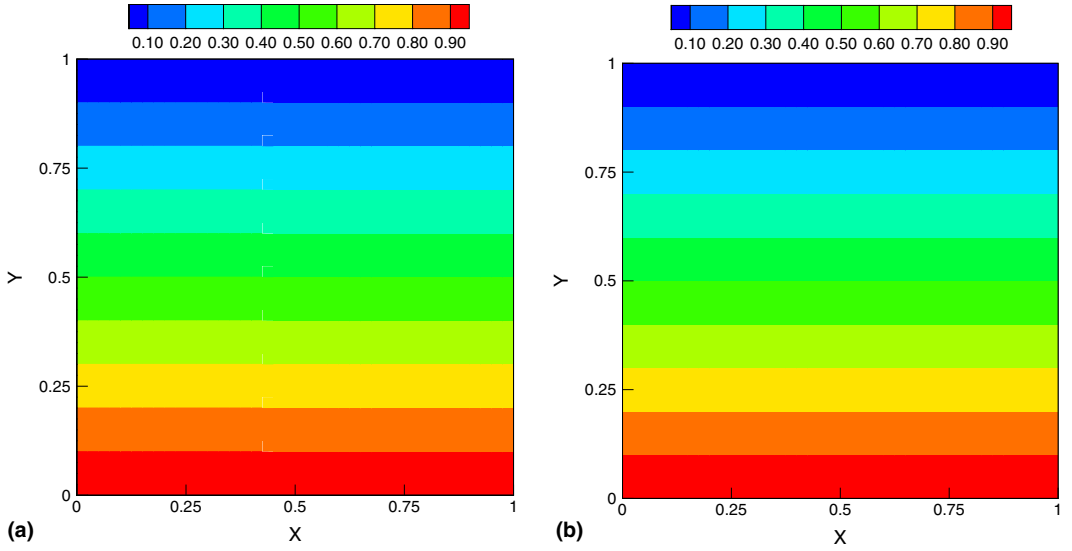

Fig. 10. Example II: (a) mean non-dimensional temperature at steady state for deterministic simulation at $Ra = 1530$; (b) prediction of support-space method for non-dimensional temperature at steady state at $Ra = 1530$.

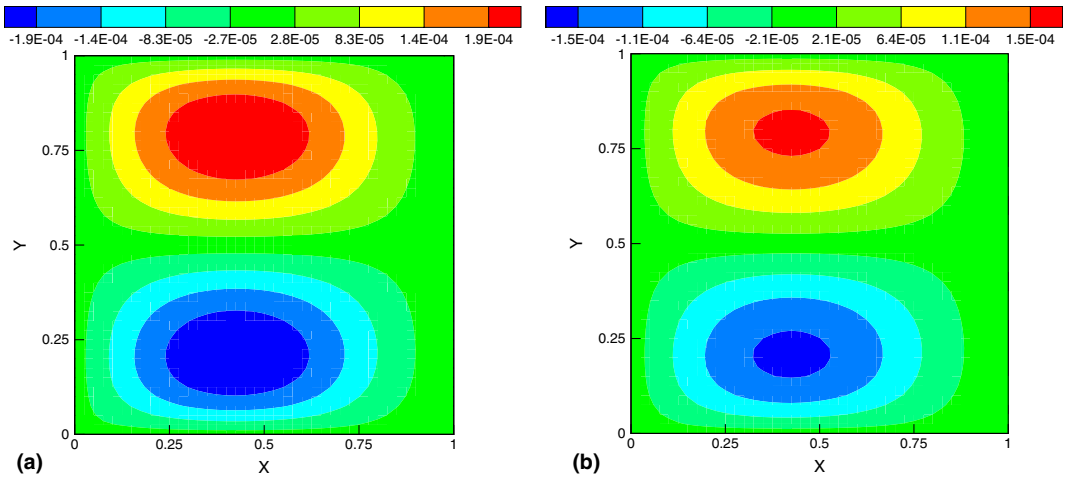

Fig. 11. Example II: (a) mean non-dimensional x-velocity component at steady state for deterministic simulation at $Ra = 1530$; (b) prediction of support-space method for non-dimensional x-velocity component at steady state at $Ra = 1530$.

variable with mean 1700, we hope to capture the system behavior on either side of the CP1. In particular, we assume the following uniform distribution model for the Rayleigh number:

$$Ra = Ra_c(1 + 0.1\xi), \quad \xi \overset{d}{=} U[-1, 1], \quad Ra_c = 1700.$$

This model corresponds to 10% fluctuation in Rayleigh number about the critical value. A 40-by-40 mesh comprising of bilinear quadrilateral elements was used to discretize the spatial domain. Owing to the uniform PDF model for the Rayleigh number, ten elements were sufficient to discretize the support-space.

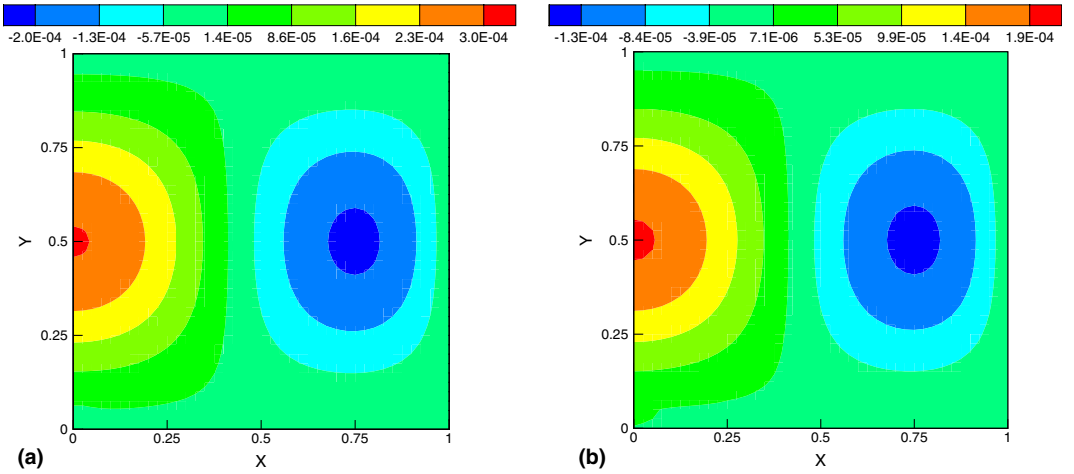

Fig. 12. Example II: (a) mean non-dimensional y-velocity component at steady state for deterministic simulation at $Ra = 1530$; (b) prediction of support-space method for non-dimensional y-velocity component at steady state at $Ra = 1530$.

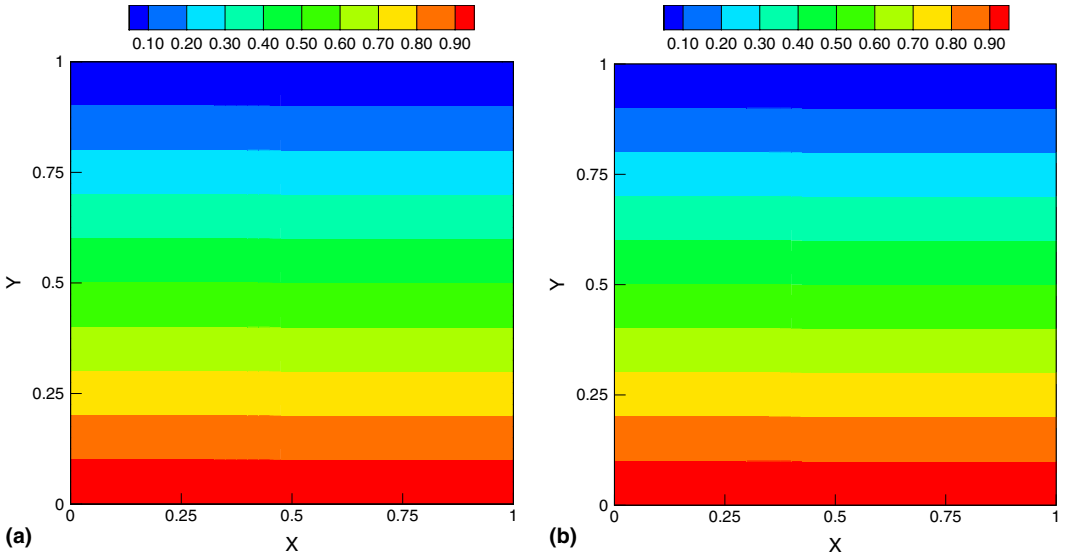

Fig. 13. Example II: (a) mean non-dimensional temperature at steady state for deterministic simulation at $Ra = 1870$; (b) prediction of support-space method for non-dimensional temperature at steady state at $Ra = 1870$.

For the sake of comparison with the GPCE approach, we consider a third-order Legendre-chaos expansion for the solution temperature and flow fields. The temperature boundary condition on the cold wall is $\theta_C = 0$ and the temperature conditions at the hot wall are prescribed as follows (for the GPCE approach):

$$\theta_0|_{\text{hot}} = 1, \quad \theta_r|_{\text{hot}} = 0, \quad r = 1, 2, 3. \tag{57}$$

In addition to the above two stochastic analysis approaches, we also consider two deterministic simulation runs for Rayleigh numbers 1530 and 1870. These correspond to the two extreme values that the Rayleigh number can take. The velocity contours for the simulation at $Ra = 1530$ and the simulation at $Ra = 1870$ can be thought of as lower and upper bounds of the flow velocity.

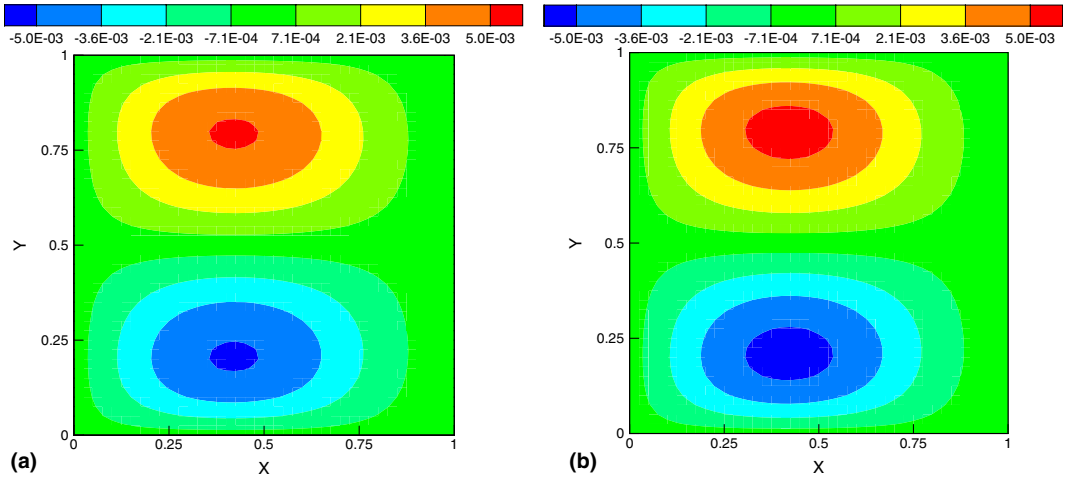

Fig. 14. Example II: (a) mean non-dimensional x-velocity component at steady state for deterministic simulation at $Ra = 1870$; (b) prediction of support-space method for non-dimensional x-velocity component at steady state at $Ra = 1870$.

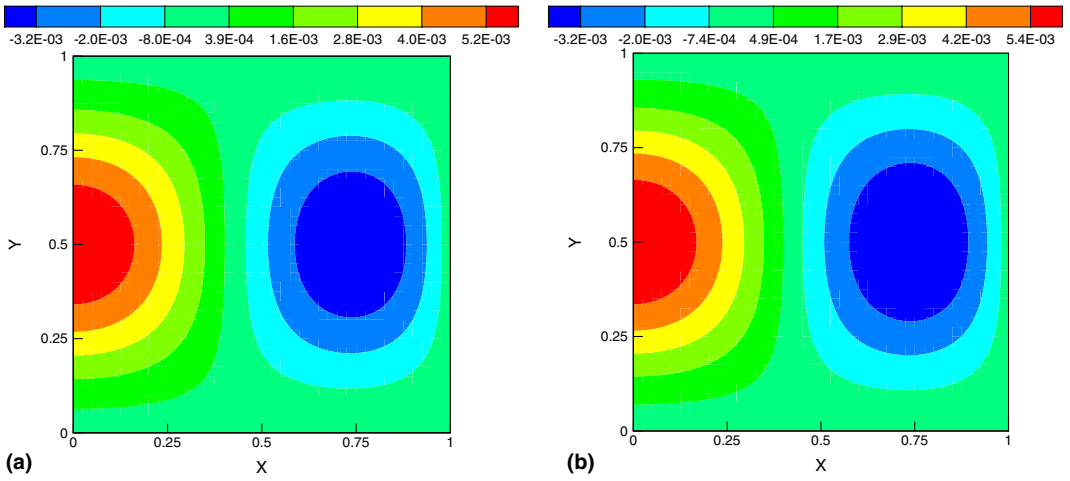

Fig. 15. Example II: (a) mean non-dimensional y-velocity component at steady state for deterministic simulation at $Ra = 1870$; (b) prediction of support-space method for non-dimensional y-velocity component at steady state at $Ra = 1870$.

(A) *GPCE approach – steady-state results and discussion*: The various results obtained for this simulation near CP1 are summarized in Figs. 9–15. The GPCE approach does not provide satisfactory results even for the steady-state mean velocity contours. This can be observed by viewing Figs. 9(a) and (b). The mean velocity values must lie between the velocity values obtained for the two extreme Rayleigh numbers in Figs. 11(a) and 14(a). This argument holds since, at the lower extreme Rayleigh number, the flow is absent and at the higher extreme Rayleigh number, the flow velocity is maximum. The GPCE however predicts an incorrect near-zero mean velocity. This points to the failure of the method. Since, the prediction for mean velocity is incorrect, we do not provide the higher order velocity statistics.

(B) *Support space approach – steady-state results and discussion*: A relatively coarse support-space (interval $[-1,1]$) grid comprising of ten equal linear elements was used. Even for this grid, the predictions of velocity at the two extreme Rayleigh numbers is fairly accurate. Further, the method has an added advantage that we can obtain the flow and temperature patterns (L_2 estimates) at any intermediate Rayleigh number by simple finite element interpolation. Thus, a single stochastic simulation can hold readily available information of millions of deterministic simulations at slightly higher computation cost.

The comparisons between the prediction of the support-space method and the deterministic simulation at a Rayleigh number of 1530 are shown in Figs. 10(a)–12(a). The comparisons between the prediction of the support-space method and the deterministic simulation at a Rayleigh number of 1870 are shown in Figs. 13–15.

We also wish to comment on similar results obtained in [8], where the authors used Wiener–Haar expansion with 32 degrees of freedom to discretize the support space. The method introduced in this work gives comparable accuracy for one-third of the discretization level used in [8].

7. Summary

The paper presents a stabilized stochastic finite element implementation for the solution of natural convection system of equations with uncertainty in initial conditions, boundary conditions and/or fluid properties. The stabilized formulations are derived using the variational multiscale framework. In particular two kinds of problems were considered:

- Problem I. *Simulation of natural convection far from critical points*: Here, the GPCE approach was considered owing to its exponential convergence properties.
- Problem II. *Simulation of natural convection wherein the inputs fluctuations are such that the system can be above and below CP1 with finite probabilities*: Here, the GPCE approach fails due to the highly non-linear uncertainty propagation. An alternative support-space approach is devised to successfully address this problem.

The salient features of the support-space approach in comparison with the GPCE approach as detected in the results of the numerical experiments are as follows:

- The support-space approach incurs a larger computation cost (about a factor of 2^d, where d is the KL dimension of the input) in comparison to the GPCE approach for a given stochastic simulation of systems away from critical points.
- Though the support-space approach gives a fairly accurate estimate of the system output near critical points, significant research still remains to be done for the method to become a powerful alternative approach to repeated deterministic simulations as in Monte Carlo techniques.
- Both the GPCE and the support-space method can be easily integrated using a deterministic finite element code with a few modifications.

- The support-space approach can handle completely empirical probability density functions with no change in the convergence properties (convergence is based on number of elements used to discretize the support-space). GPCE on the other hand looses its convergence properties if the Askey chaos chosen does not correspond to the input distribution.

Acknowledgements

The work presented here was funded in part by NASA, Office of Biological and Physical Sciences Research (Grant No. NAG8-1671) and the Computational Mathematics Program of the Air Force Office of Scientific Research (Grant No. FA9550-04-1-0070). This research was conducted using the resources of the Cornell Theory Center, which receives funding from Cornell University, New York State, federal agencies, and corporate partners.

References

[1] S. Chandrasekhar, Hydrodynamic and Hydromagnetic Stability, Clarendon Press, Oxford, 1961.
[2] W. Schoutens, Stochastic processes and orthogonal polynomialsLecture Notes in Statistics, vol. 146, Springer-Verlag, New York, 2000.
[3] D. Xiu, D. Lucor, C.-H. Su, G.E. Karniadakis, Stochastic modeling of flow-structure interactions using generalized polynomial chaos, J. Fluids Eng. 125 (2001) 51–59.
[4] M. Jardak, C.-H. Su, G.E. Karniadakis, Spectral polynomial chaos solutions of the stochastic advection equation, J. Sci. Comput. 17 (2002) 319–338.
[5] D. Xiu, G.E. Karniadakis, Modeling uncertainty in flow simulations via generalized polynomial chaos, J. Comput. Phys. 187 (2003) 137–167.
[6] O.P. Le Maitre, O.M. Kino, H.N. Najm, R. Ghanem, A stochastic projection method for fluid flow I. Basic formulation, J. Comput. Phys. 173 (2001) 481–511.
[7] O.P. Le Maitre, M. Reagan, H.N. Najm, R. Ghanem, O.M. Knio, A stochastic projection method for fluid flow. II: Random process, J. Comput. Phys. 181 (2002) 9–44.
[8] O.P. Le Maitre, O.M. Knio, H.N. Najm, R.G. Ghanem, Uncertainty propagation using Wiener–Haar expansions, J. Comput. Phys. 197 (1) (2004) 28–57.
[9] M.K. Deb, I.M. Babuska, J. Tinsley Oden, Solution of stochastic partial differential equations using Galerkin finite element techniques, Comput. Meth. Appl. Mech. Eng. 190 (2001) 6259–6372.
[10] B. Velamur Asokan, N. Zabaras, Variational multiscale stabilized FEM formulations for transport equations: stochastic advection-diffusion and incompressible stochastic Navier–Stokes equations, J. Comput. Phys. 202 (2005) 94–133.
[11] T.J.R. Hughes, Multiscale phenomena: Green's functions, the Dirichlet-to-Neumann formulation, subgrid scale models, bubbles and the origin of stabilized methods, Comput. Meth. Appl. Mech. Eng. 127 (1995) 387–401.
[12] J.-L. Guermond, Stabilization of Galerkin approximations of transport equations by subgrid modeling, M2AN 33 (1999) 1293–1316.
[13] T.J.R. Hughes, L. Mazzei, K.E. Jansen, Large eddy simulation and the variational multiscale method, Comput. Visual. Sci. 3 (2000) 47–59.
[14] S.I. Resnick, A Probability Path, Birkhäuser, Boston, USA, 2001.
[15] M. Loève, Probability Theory, fourth ed., Springer-Verlag, Berlin, 1977.
[16] R.G. Ghanem, P.D. Spanos, Stochastic Finite Elements: A Spectral Approach, Springer-Verlag, 1991.
[17] N. Wiener, The homogenous chaos, Am. J. Math. 60 (1938) 897–936.
[18] R.H. Cameron, W.T. Martin, The orthogonal development of non-linear functionals in series of Fourier Hermite functionals, Ann. Math. 48 (1947) 385–392.
[19] R. Codina, Stabilized finite element approximation of transient incompressible flows using orthogonal subscales, Comput. Meth. Appl. Mech. Eng. 191 (39–40) (2002) 4295–4321.
[20] R. Codina, Analysis of a stabilized finite element approximation of the transient convection-diffusion equation using orthogonal subscales, Comput. Visual. Sci. 4 (3) (2002) 167–174.
[21] M.Y. Ha, I.-K. Kim, H.S. Yoon, S. Lee, Unsteady fluid-flow and temperature fields in a horizontal enclosure with an adiabatic body, Phys. Fluids 14 (9) (2002) 3189–3202.